

Figure 2. Phase diagram for $\tilde{\rho}$ in the $(N, \tilde{\sigma}_0)$ -plane. In the QHS phase $\tilde{\rho}_{xx} \gg \tilde{\rho}_{yy}$, while in the hQHS, AU, and CZS phases $\tilde{\rho}_{xx} = \tilde{\rho}_{yy}$. Numbers in parentheses label equations for $\tilde{\rho}$ in corresponding phases. Thick boundaries mark destruction of stripe phases. N_q and $\tilde{\sigma}_q$ are given by Eqs. (13) and (14), respectively. We used $n_e = 3 \times 10^{11} \text{ cm}^{-3}$, $\gamma = 0.53$, and quantum lifetime $\tau_q = 75 \text{ ps}$.

QHS phase. Combining Eq. (1) and Eq. (36) in Ref. 8, $(\tilde{\rho}_{xx}\tilde{\rho}_{yy})^{1/2} \simeq 1/8N^2$, we find

$$\tilde{\rho}_{xx} \simeq \frac{\tilde{\sigma}_0}{64\gamma\alpha^2 N^4}, \quad (2)$$

$$\tilde{\rho}_{yy} \simeq \frac{\gamma\alpha^2}{\tilde{\sigma}_0}. \quad (3)$$

For a given $\tilde{\sigma}_0$ the “hard” $\tilde{\rho}_{xx}$ scales with N^{-4} whereas the “easy” $\tilde{\rho}_{yy}$ is N -independent. The border between the QHS and hQHS phases in Figure 2 is determined by the condition $\tilde{\rho}_{xx} = \tilde{\rho}_{yy}$ and can be written as

$$\tilde{\sigma}_0 = 8\gamma\alpha^2 N^2, \quad (4)$$

i.e., the QHS phase should cease at $N = \sqrt{\tilde{\sigma}_0/8\gamma\alpha^2}$.

hQHS phase. We show below that the hQHS resides between its upper border, Eq. (4), and its lower border,

$$\tilde{\sigma}_0 \approx 3.5\gamma\alpha^2 N. \quad (5)$$

To find $\tilde{\rho}(N, \tilde{\sigma}_0)$, we start with Eqs. (38) and (39) in Ref. 12

$$\tilde{\sigma} = \frac{h v_F^2 g_B \tau_B}{2(1 + \omega_c^2 \tau_B^2)} = \frac{\tilde{\sigma}_0}{2\gamma(1 + \omega_c^2 \tau_B^2)}, \quad (6)$$

where

$$\frac{1}{\tau_B} = \frac{\gamma g_B}{\tau g_0}. \quad (7)$$

Here, the scattering time τ_B and the DOS at the center of the Landau level g_B are both at magnetic field, while the Fermi velocity v_F and the DOS per spin $g_0 = m^*/2\pi\hbar^2$ are at $B = 0$. The coefficient $\gamma < 1$ reflects a stronger need for momentum transfer for the rate $1/\tau_B$ of hops between stripe edges in the

hQHS phase than for Ref. 12 hops in a uniform 2DEG where $\gamma = 1$ [13].

In the hQHS phase, $g_B = \alpha g_0$ [9], and following Eq. (5) we have the double inequality $\tilde{\sigma}_0 \gg \gamma\alpha^2 N \gg \alpha N$. Therefore $\omega_c \tau_B = \tilde{\sigma}_0/2\gamma\alpha N \gg 1$, and Eq. (6) yields

$$\tilde{\sigma} \simeq \frac{2\gamma\alpha^2 N^2}{\tilde{\sigma}_0}. \quad (8)$$

Also the same double inequality implies $\tilde{\sigma} \ll \tilde{\sigma}_H \simeq 2N$, and we arrive at

$$\tilde{\rho} \simeq \frac{\tilde{\sigma}}{\tilde{\sigma}_H^2} \simeq \frac{\gamma\alpha^2}{2\tilde{\sigma}_0}, \quad (9)$$

which is two times smaller than Eq. (3). The independence of $\tilde{\rho}$ on N and its inverse proportionality to $\tilde{\sigma}_0$ are the hallmarks of the hQHS phase.

AU phase. Using $\tilde{\sigma} = 2N/\pi$ calculated in Ref. 10 for low mobility samples with $\tau = \tau_q$ and $\tilde{\sigma}_H \simeq 2N$ we find

$$\tilde{\rho} = \frac{\tilde{\sigma}}{\tilde{\sigma}^2 + \tilde{\sigma}_H^2} \simeq \frac{0.14}{N}. \quad (10)$$

This parameter-free result matches Eq. (9) at the upper border of AU phase given by Eq. (5) and is shown in Figure 2.

CZS phase. To find $\tilde{\rho}$ in the CZS phase in samples with $\tau \gg \tau_q$, we calculate τ_B using Eq. (6) with $g_B = g_0\sqrt{\omega_c\tau_q}$ [11, 14, 15]. We also use $\gamma = 1$ because stripes are destroyed. Combining this with $\omega_c \tau_B \sim \sqrt{\omega_c \tau^2/\tau_q} \gg 1$ Eq. (6) gives [12]

$$\tilde{\sigma} \simeq \frac{\tau_q}{\tau} N, \quad (11)$$

which has an extra factor of $\pi\tau_q/2\tau$ compared to $\tilde{\sigma} = 2N/\pi$ in the AU phase [10]. For $\tau_q/\tau \ll 1$, we have $\tilde{\sigma} \ll \tilde{\sigma}_H$ and

$$\tilde{\rho} \simeq \frac{\tilde{\sigma}}{\tilde{\sigma}_H^2} = \frac{1}{4} \frac{\tau_q}{\tau} \frac{1}{N}. \quad (12)$$

This agrees with Eq. (6) in Ref. 11. Equation (12) matches $\tilde{\rho}$ in the AU phase, Eq. (10), at $\tau \simeq 1.7\tau_q$ or at

$$\tilde{\sigma}_0 \approx 1.7\tilde{\sigma}_q, \quad \tilde{\sigma}_q \equiv \frac{h n_e \tau_q}{m^*}. \quad (13)$$

Eq. (12) also matches $\tilde{\rho}$ in the hQHS phase, Eq. (9), at

$$N \approx N_q \equiv \frac{h n_e \tau_q}{2\gamma\alpha^2 m^*}. \quad (14)$$

This equation allows one to find τ_q using experimental N_q .

To construct the phase diagram Figure 2, we used Eqs. (4), (5), (13), and (14) with $n_e = 3 \times 10^{11} \text{ cm}^{-3}$, $\gamma = 0.53$ calculated in Appendix, and $\tau_q = 75 \text{ ps}$ [16].

Using these numbers, we have in mind a series of samples with approximately the same n_e and widely varying mobility and $\tilde{\sigma}_0$, which are made of very high mobility GaAs quantum wells by replacing small and varying fraction x of Ga

atoms by Al [17]. In these samples, the short range Al impurities determine τ and τ_B , while τ_q is determined by scattering on Coulomb background impurities and remote donors and, therefore, is independent on x [18].

Let us now discuss predictions of our phase diagram Figure 2 for $\tilde{\rho}(N)$ of three hypothetical samples with $\tilde{\sigma}_0 = 10^3, 3 \times 10^3$ and 10^4 . The first sample at all N should reside in the AU phase and, therefore, obey Eq. (10). The second one at $N \leq 5$ should be in the hQHS phase and, therefore, its $\tilde{\rho}(N)$ should be given by Eq. (9) and be independent on N . This plateau should end at $N > 5$, where $\tilde{\rho}(N)$ should start declining as $1/N$ according to Eq. (10). Finally the third sample at $N = 2$ should show anisotropic $\tilde{\rho}(N)$, then between $N = 3$ and $N = N_q = 7$, show a plateau $\tilde{\rho}(N)$, and eventually at $N > 7$ should follow Eq. (12) of the CZS phase. Such a diversity of $\tilde{\rho}(N)$ dependencies is a consequence of predicted in this paper the hidden stripe phase. If such $\tilde{\rho}(N)$ are observed experimentally in samples, one should be able to find τ_q from experimental value of N_q .

So far we dealt only with half-integer ν . Let us conclude by commenting on the fate of bubble phases, generalizations of Wigner crystals with $M \geq 2$ electrons per unit cell [1, 2, 19–22], which emerge when ν is detuned from half-integer by $\gtrsim \pm 0.1$. Due to pinning of bubble crystals they are usually detected via intervals of ν where $\rho_{xx} = 0$ in flanks of central half-integer peaks. Since only the DOS governs this isotropic regime, the hQHS resistance peaks also include hidden bubbles, which have comparable DOS not too far away from half-filling. As a result, in hQHS phase the resistance peaks broaden and acquire the shape similar to that in the AU phase, widely discussed in literature [10, 23].

We thank I. Dmitriev, M. Fogler, and X. Fu for valuable discussions. Calculations by Y. H. and M. S. were supported primarily by the NSF through the University of Minnesota MRSEC under Award No. DMR-1420013. M. Z. acknowledges support from the U.S. Department of Energy, Office of Science, Basic Energy Sciences, under Award No. DE-SC0002567.

* Corresponding author: huan1756@umn.edu

Supplementary material: calculation of γ for scattering dominated by short-range (Al) impurities

In this subsection we assume that the Al impurities dominate the scattering rates $1/\tau$ and $1/\tau_B$. Let us start with the scattering rate in zero magnetic field

$$\frac{1}{\tau} = \frac{2\pi}{\hbar} \sum_f \langle |U_{fi}|^2 \rangle \delta(\epsilon_f - \epsilon_i) (1 - \cos \theta), \quad (\text{S15})$$

- [1] A. A. Koulakov, M. M. Fogler, and B. I. Shklovskii, *Phys. Rev. Lett.* **76**, 499 (1996).
- [2] M. M. Fogler, A. A. Koulakov, and B. I. Shklovskii, *Phys. Rev. B* **54**, 1853 (1996).
- [3] R. Moessner and J. T. Chalker, *Phys. Rev. B* **54**, 5006 (1996).
- [4] C. Wexler and A. T. Dorsey, *Phys. Rev. B* **64**, 115312 (2001).
- [5] E. H. Rezayi, F. D. M. Haldane, and K. Yang, *Phys. Rev. Lett.* **83**, 1219 (1999).
- [6] M. P. Lilly, K. B. Cooper, J. P. Eisenstein, L. N. Pfeiffer, and K. W. West, *Phys. Rev. Lett.* **82**, 394 (1999).
- [7] R. R. Du, D. C. Tsui, H. L. Stormer, L. N. Pfeiffer, K. W. Baldwin, and K. W. West, *Solid State Commun.* **109**, 389 (1999).
- [8] A. H. MacDonald and M. P. A. Fisher, *Phys. Rev. B* **61**, 5724 (2000).
- [9] M. Sammon, X. Fu, Y. Huang, M. A. Zudov, B. I. Shklovskii, G. C. Gardner, J. D. Watson, M. J. Manfra, K. W. Baldwin, L. N. Pfeiffer, and K. W. West, *Phys. Rev. B* **100**, 241303 (2019).
- [10] T. Ando and Y. Uemura, *J. Phys. Soc. Jpn.* **36**, 959 (1974).
- [11] P. T. Coleridge, P. Zawadzki, and A. S. Sachrajda, *Phys. Rev. B* **49**, 10798 (1994).
- [12] I. A. Dmitriev, A. D. Mirlin, D. G. Polyakov, and M. A. Zudov, *Rev. Mod. Phys.* **84**, 1709 (2012).
- [13] Our Eq. (6) has a factor 1/2 compared to Eq. (39) of Ref. 12 because we deal with spin resolved LLs. Also note that τ_B is one half the τ_B defined in Ref. 9.
- [14] M. E. Raikh and T. V. Shahbazyan, *Phys. Rev. B* **47**, 1522 (1993).
- [15] A. D. Mirlin, E. Altshuler, and P. Wölfle, *Ann. Phys.* **5**, 281 (1996).
- [16] Q. Shi, M. A. Zudov, I. A. Dmitriev, K. W. Baldwin, L. N. Pfeiffer, and K. W. West, *Phys. Rev. B* **95**, 041403(R) (2017).
- [17] G. C. Gardner, J. D. Watson, S. Mondal, N. Deng, G. A. Csáthy, and M. J. Manfra, *Appl. Phys. Lett.* **102**, 252103 (2013).
- [18] M. Sammon, M. A. Zudov, and B. I. Shklovskii, *Phys. Rev. Materials* **2**, 064604 (2018).
- [19] K. B. Cooper, M. P. Lilly, J. P. Eisenstein, L. N. Pfeiffer, and K. W. West, *Phys. Rev. B* **60**, 11285 (1999).
- [20] J. P. Eisenstein, K. B. Cooper, L. N. Pfeiffer, and K. W. West, *Phys. Rev. Lett.* **88**, 076801 (2002).
- [21] X. Fu, Q. Shi, M. A. Zudov, G. C. Gardner, J. D. Watson, and M. J. Manfra, *Phys. Rev. B* **99**, 161402 (2019).
- [22] D. Ro, N. Deng, J. D. Watson, M. J. Manfra, L. N. Pfeiffer, K. W. West, and G. A. Csáthy, *Phys. Rev. B* **99**, 201111(R) (2019).
- [23] T. Ando, A. B. Fowler, and F. Stern, *Rev. Mod. Phys.* **54**, 437 (1982).

where U_{fi} is the matrix element of the potential U between the final and initial states, θ is the scattering angle, and $\langle \dots \rangle$ denotes averaging over disorder realizations. We first calculate

$$\langle |U_{fi}|^2 \rangle = \int d^3r d^3r' \psi_f^*(\mathbf{r}) \psi_i(\mathbf{r}) \psi_f(\mathbf{r}') \psi_i^*(\mathbf{r}') \langle U(\mathbf{r}) U(\mathbf{r}') \rangle, \quad (\text{S16})$$

where $\psi_{f,i}(\mathbf{r})$ are the wavefunctions. Using a short-range potential $U(\mathbf{r}) = \sum_l (U_0 a^3) \delta^3(\mathbf{r} - \mathbf{r}_l)$ with the strength U_0 , the range a , and the position of the l -th impurity \mathbf{r}_l , we have the correlator after averaging over the impurities position

$$\langle U(\mathbf{r}) U(\mathbf{r}') \rangle = (U_0 a^3)^2 \left\langle \sum_{kl} \delta^3(\mathbf{r} - \mathbf{r}_k) \delta^3(\mathbf{r}' - \mathbf{r}_l) \right\rangle = (U_0 a^3)^2 N_3 \delta^3(\mathbf{r} - \mathbf{r}'). \quad (\text{S17})$$

where N_3 is the concentration of impurities. We write the final and initial states as a product of the two-dimensional plane waves with wave vector $\mathbf{k}_{f,i}$ parallel to the quantum well and the first subband bound state in the z direction $\phi(z) = (2/w)^{1/2} \sin(\pi z/w)$ where w is the well width. As a result, $\langle |U_{fi}|^2 \rangle = 3N_3 (U_0 a^3)^2 / 2wA$. Using $\sum_f \rightarrow A \int \frac{d^2 k_f}{(2\pi)^2}$ where $A = L_x L_y$ is the area of the system, we arrive at

$$\frac{1}{\tau} = \frac{2\pi}{\hbar} \frac{3N_3}{2w} (U_0 a^3)^2 \int \frac{d^2 k_f}{(2\pi)^2} \delta(\epsilon_f - \epsilon_i) (1 - \cos \theta) = \frac{2\pi}{\hbar} g_0 \frac{3N_3}{2w} (U_0 a^3)^2, \quad (\text{S18})$$

where $g_0 = m^*/2\pi\hbar^2$ is the DOS per spin at zero magnetic field.

The scattering rate in a magnetic field can be evaluated similarly, but noticing that the final and initial states become the eigenstates of the N -th LL. In the Landau gauge $\mathbf{A} = xB\hat{\mathbf{j}}$, we have

$$\psi_{f,i}(\mathbf{r}) = \phi(z) \exp(iyX_{f,i}/l_B^2) \chi_N(x - X_{f,i}) / \sqrt{L_y}, \quad (\text{S19})$$

$$\chi_N(x) = (\pi^{1/4} \sqrt{2^N N! l_B})^{-1} \exp(-x^2/2l_B^2) H_N(x/l_B), \quad (\text{S20})$$

where $X_{f,i}$ are the x coordinates of the cyclotron center of the final and initial states respectively, and L_y is the length of the sample along y direction. Eq. (S16) becomes

$$\langle |U_{fi}|^2 \rangle = \frac{3N_3}{2wA} (U_0 a^3)^2 \sum_{\mathbf{q}} \left| \int d^2r \psi_f^*(\mathbf{r}) e^{-i\mathbf{q}\cdot\mathbf{r}} \psi_i(\mathbf{r}) \right|^2 = \frac{3N_3}{2wA} (U_0 a^3)^2 \sum_{\mathbf{q}} \left(\Phi_N^2(ql_B) \delta_{q_y, X_f/l_B^2} \right), \quad (\text{S21})$$

where in the first step we use $A\delta^2(\mathbf{r} - \mathbf{r}') = \sum_{\mathbf{q}} e^{-i\mathbf{q}\cdot(\mathbf{r}-\mathbf{r}')}$ and \mathbf{q} is a 2D wave vector. In the second step, without loss of generality, we assume $X_i = 0$ and have

$$\int d^2r \psi_f^*(\mathbf{r}) e^{-i\mathbf{q}\cdot\mathbf{r}} \psi_i(\mathbf{r}) = \delta_{q_y, X_f/l_B^2} \exp(-iq_x X_f/2) \Phi_N(ql_B), \quad (\text{S22})$$

where $\Phi_N(x)$ is defined as

$$\Phi_N(x) = \exp(-x^2/4) L_N(x^2/2), \quad (\text{S23})$$

and $L_N(x)$ is the N -th Laguerre polynomial.

To sum over the contributions from final states, we make the following observations. First, the energy of final states is $\epsilon_f = V(x)$, where $V(x)$ is the stripe potential shown as Figure 1 in the main text, while the initial energy ϵ_i is zero. Thus, $\delta(\epsilon_f - \epsilon_i) = (eE)^{-1} [\delta(x - \Lambda/2) + \delta(x + \Lambda/2)]$, where we assumed that the electron can scatter only to an adjacent stripe edge, as shown in Figure 3, and used $dV/dx = eE$ with the effective electric field E . Second, since the LL degeneracy is $A/2\pi l_B^2$ and the degree of freedom of a final state is the x coordinate of its cyclotron orbit center X_f , we can make a substitution $\sum_f \rightarrow L_y/2\pi l_B^2 \int dX_f$. Third, in continuous limit $\sum_{q_x} \rightarrow L_x \int dq_x/2\pi$ and, as a result,

$$\frac{1}{\tau_B} = \frac{2\pi}{\hbar} g_B \frac{3N_3}{2w} (U_0 a^3)^2 \Lambda \int \frac{dq_x}{2\pi} \Phi_N^2(ql_B), \quad (\text{S24})$$

where $q = \sqrt{q_x^2 + \Lambda^2/4l_B^4}$, $g_B = 2(2\pi l_B^2 eE\Lambda)^{-1}$ is the DOS in magnetic field. Comparing Eq. (S24) to Eq. (S18) and using Eq. (5) in the main text we find

$$\gamma = \Lambda \int_{-\infty}^{\infty} \frac{dq_x}{2\pi} \Phi_N^2(ql_B) = \Lambda \int_{-\infty}^{\infty} dx \chi_N^2(x) \chi_N^2(x - \Lambda/2), \quad (\text{S25})$$

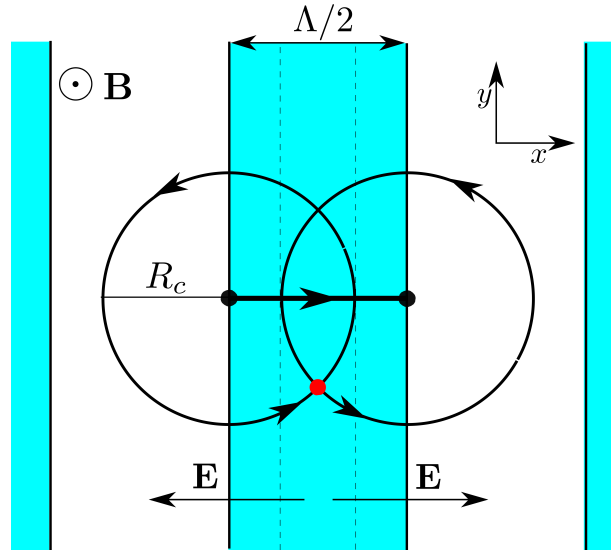


Figure 3. Schematic of transport in the stripe phase. Electrons on the stripe edges drift in electric fields E in the $\pm y$ -direction. They are scattered to an adjacent stripe edge by Al impurities at a rate $1/\tau_B$, as illustrated by thick horizontal arrow. The impurities which can scatter electrons between stripe edges reside in a narrow strip between dashed lines. Example of such an impurity is shown by a red dot.

where $\chi_N(x)$ is defined by Eq. (S20). At large N , $\chi_N^2(x)$ is just the classical probability distribution of a particle in a parabolic potential:

$$\lim_{N \rightarrow \infty} \chi_N^2(x) = \frac{\Theta(R_c - |x|)}{\pi \sqrt{R_c - x}}. \quad (\text{S26})$$

Therefore, $\chi_N^2(x)$ and $\chi_N^2(x - \Lambda/2)$ of electrons residing at adjacent stripe edges overlap practically only within a narrow strip whose boundaries are marked by dashed lines in Figure 3. This strip has a width $2R_c - \Lambda/2$ and covers $\sim 40\%$ of the area between two edges. Therefore, only about 40% of impurities contribute to scattering. However, since both $\chi_N^2(x)$ and $\chi_N^2(x - \Lambda/2)$ peak within the strip, $\gamma = 0.53 > 0.40$.